Multiple-Model Switching Control of Vehicle Longitudinal Dynamics for Platoon-Level Automation

Shengbo Eben Li, *Member, IEEE*, Feng Gao, Dongpu Cao, and Keqiang Li

***Abstract*—Platooning of autonomous vehicles has the potential to significantly benefit road traffic. This paper presents a new robust acceleration tracking control of vehicle longitudinal dynamics toward platoon-level automation. Based on a multiple-model switching structure, this design divides the large uncertainties of vehicle dynamics into small uncertainties and, accordingly, develops multiple robust controllers for the multiple-model set. The switching control system automatically selects the most appropriate candidate controller into the loop, according to the errors between current vehicle dynamics and multiple models. This technique offers more consistent and approximately linear node dynamics for upper level platoon control, even under relatively large vehicle uncertainties. Simulation comparison with a sliding model controller and a fixed H-infinity controller is conducted for a passenger car to demonstrate the enhanced robustness of the switching control method. The experimental test for the same car is performed for further validation.**

***Index Terms*—Acceleration control, autonomous vehicle, multiple-model switching (MMS), platoon control.**

I. Introduction

THE platooning of autonomous vehicles has considerable potential for benefiting road traffic, including increased highway capacity, less fuel/energy consumption, and, hopefully, fewer accidents [1]. The process of platooning has been accelerated with increasing usage of wireless communication in road transportation [2]. Pioneering studies on platoon control can date back to 1990s [3], [4]. As pointed out by Hedrick and Tomizuka *et al.*, the control topics of a platoon can be divided into two tasks: 1) to implement control of platoon formation, stabilization, and dissolution and 2) to carry out controls for throttle/brake actuators of each vehicle [5]. These naturally lead to a hierarchical control structure, including upper level control and lower level control [6]–[8], in which the upper level control retains safe and string stable operation, whereas lower level control tracks the desired acceleration by determining throttle/brake commands.

The upper level control of platoons has been extensively investigated. An earlier work done by Shladover introduced many known control topics, among which the most famous is the concept of string stability [3]. String stability ensures that range errors decrease as propagating along downstream [9]. Rajamani *et al.* designed a sliding mode controller to achieve string-stable car-following, whereas the intraplatoon behaviors were discussed considering the request of drivers to execute split and joint maneuvers [6]. Stankovic and Stanojevic proposed a decentralized overlapping control law by using the inclusion principle, which decomposes the original system into multiple systems by an appropriate input/state expansion [10]. Up to now, many upper level topics have been explored, including the influence of spacing policies, information flow topologies, and time delay in communication systems.

Lower level control, which is also called acceleration tracking control, determines the commands for the throttle and/or brake actuators. The lower level controller, together with the vehicle itself, actually plays the role of node dynamics for upper level control. Many research efforts have been attempted on acceleration control in the past decades, but still, few gives emphasis on the request of platoon-level automation. Most platoon control relies on one important assumption that the node dynamics are homogeneous and approximately linear. Then, the node dynamics can be described to simple models, e.g., a double-integrator model [12], [13] and a three-order model [4], [6], [9]–[11]. This requires the behavior of acceleration control to be rather accurate and consistent, but difficult to be achieved. One reason is that the salient nonlinearities in powertrain dynamics, both traditional [14], [15] and hybridized [16], [17], and any linearization will lead to large errors; another reason is that such uncertainties as parametric variation and external disturbances significantly alter the consistence of control behavior.

The major issues of acceleration tracking control are how to deal with nonlinearities and uncertainties. For the nonlinearities, the majority now is to linearize powertrain dynamics, including exact linearization [18], [19], Taylor linearization [20], and inverse model compensation [14], [15]. Fritz and Schiehlen uses the exact linearization technique to normalize node dynamics for cruising control [18], [19]. After linearization, a pole placement controller was employed to control

Manuscript received January 19, 2015; revised September 26, 2015 and December 24, 2015; accepted February 19, 2016. Date of publication March 11, 2016; date of current version June 16, 2016. This work was supported in part by the National Natural Science Foundation of China under Grant 51575293 and in part by the State Key Laboratory of Automotive Safety and Energy under Grant KF16192. The review of this paper was coordinated by Dr. S. Anwar. *(Corresponding author: Feng Gao.)*

S. E. Li and K. Li are with the State Key Laboratory of Automotive Safety and Energy, Department of Automotive Engineering, Tsinghua University, Beijing 100084, China (e-mail: lisb04@gmail.com; likq@tsinghua.edu.cn).

F. Gao is with the School of Electrical Engineering, Chongqing University, Chongqing 400044, China (e-mail: gaofeng1@cqu.edu.cn).

D. Cao is with the Center for Automotive Engineering, Cranfield University, Cranfield MK43 0AL, U.K. (e-mail: d.cao@cranfield.ac.uk).

Color versions of one or more of the figures in this paper are available online at http://ieeexplore.ieee.org.

Digital Object Identifier 10.1109/TVT.2016.2541219

0018-9545 © 2016 IEEE. Personal use is permitted, but republication/redistribution requires IEEE permission.
See http://www.ieee.org/publications_standards/publications/rights/index.html for more information.

the exactly linearized states. The Taylor expansion has been used by Hunt to approximate the powertrain dynamics at an equilibrium point. The gain-scheduling technique was used to conquer the discrepancy caused by linearization [20]. Inverse model compensation is widely used in engineering practice, for example, in [14] and [15]. This method is implemented by neglecting the powertrain dynamics. For the uncertainties, the majority relies on robust control techniques, including sliding model control (SMC) [6], [21], H-infinity [22], [23], adaptive control [25], [26], and fuzzy control [27], [28]. A multimode SMC was designed by Rajamani to enhance control robustness [6]. Considering parametric variation, adaptive SMC was designed by Swaroop by adding an online estimation of the aerodynamic drag coefficient, vehicle mass, and rolling resistance [21]. Higashimata *et al.* and Yamamura *et al.* designed an MMC-based controller for headway control [22], [23]. The design used an H-inf controller as feedback and a forward compensator for the fastness. Xu and Ioannou approximated vehicle dynamics to be a first-order transfer function, and a Lyapunov-based design was used to derive the adaptive law [25]. Keneth *et al.* designed an adaptive proportional–integral controller for robust tracking control in resistance to parametric variation. The adaptive law is designed by using the gradient algorithm [26]. The aforementioned controller is useful to resist small errors and disturbances in vehicle longitudinal dynamics, but might not be always effective for large uncertainties. Moreover, the use of an adaptive mechanism is only able to resist slowly varying uncertainties but has difficulty responding to fast-varying disturbances, e.g., instantaneous wind.

The major purpose of this paper is to provide an accurate and consistent acceleration tracking control of vehicle longitudinal dynamics for platoon-level automation. The design, which is based on the multiple-model switching (MMS) control structure, is expected to provide approximately homogeneous and linear node dynamics for upper level control. The MMS acceleration controller has the potential to enclose the input–output behaviors of node dynamics to a specified small range even under large linearization errors and model uncertainties. The rest of this paper is organized as follows: Section II presents the vehicle model for control; Section III designs the MMS controller and proves its stability; Section IV shows the simulation comparison with two other controllers; Section V validates the effectiveness by a road test; and Section VI concludes this paper.

II. Vehicle Longitudinal Model for Control

The MMS control is an efficient way to deal with plants with large model uncertainties and linearization errors, particularly when sudden changes occur in plant dynamics [29], [30]. The overall range of plant dynamics is covered by a set of models instead of a single model, and a scheduling logic then switches the most appropriate controller into the control loop. The speed of adaptation and transient performance can be significantly improved by the instantaneous switching among candidate controllers [31], [32]. Another benefit of MMS control is its potential to enclose the input–output behaviors to a predefined range.

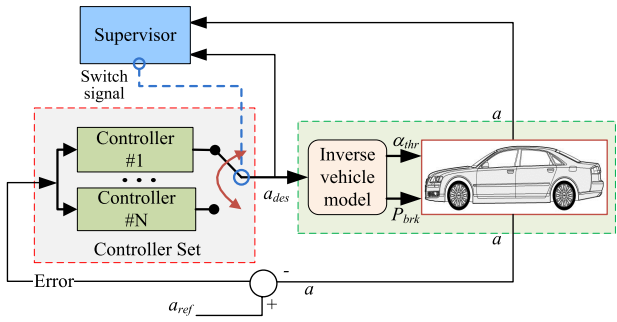

Fig. 1. MMS control configuration for vehicle acceleration tracking (a—longitudinal acceleration, $a_{\rm des}$—desired acceleration, $\alpha_{\rm thr}$—throttle angle, and $P_{\rm brk}$—braking pressure).

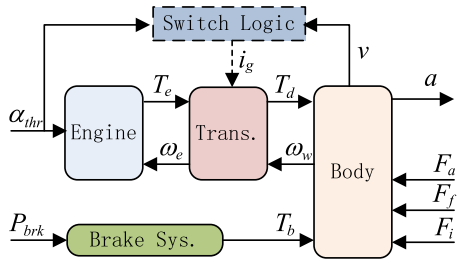

Fig. 2. Sketch of vehicle longitudinal dynamics.

Fig. 1 presents the MMS control configuration for vehicle acceleration tracking. It consists of the vehicle itself $(\mathbf{V})$, an inverse model $(\mathbf{I})$, a supervisor $(\mathbf{S})$, and a controller set $(\mathbf{C})$. The inverse vehicle model $\mathbf{I}$ is used to compensate for the powertrain nonlinearities; $\mathbf{I}$ and $\mathbf{V}$ together constructs the plant for MMS control. The combination of $\mathbf{I}+\mathbf{V}$ tends to have large uncertainties but is divided into small uncertainties under the MMS structure. Such a configuration is able to maintain more accurate and consistent performance even under a large model mismatch.

A. Nonlinearity Compensation by Inverse Vehicle Model

The vehicle for control is a passenger car with a 1.6-L gasoline engine, a torque converter (TC), a four-speed automatic transmission, two driving and two driven wheels, and a hydraulic braking system. Fig. 2 sketches the powertrain dynamics. The inputs are the throttle angle $(\alpha_{\rm thr})$ and the braking pressure $(P_{\rm brk})$. The outputs include the longitudinal acceleration (a), vehicle velocity (v), and other measurable variables in the powertrain. When driving, the engine torque is amplified by a TC, mechanical transmission, and a final gear and acts on two frontal driving wheels. When braking, the braking torque acts on four wheels to dissipate the kinetic energy of the vehicle body.

For the sake of controller design, we have the following assumptions: 1) The dynamics in intake manifold and chamber combustion are neglected, and overall powertrain dynamics are lumped into a first-order inertial transfer function; 2) the vehicle runs on dry alphabet roads with high road–tire friction, and the tire longitudinal slip is neglected; 3) the vehicle body is

TABLE I
NOMINAL PARAMETERS OF VEHICLE MODEL

Symbol	Units	Nominal value
M	kg	1300
J_e	kg·m^2	0.21
η_T	--	0.89
τ_e	sec	0.3
i_0	--	4.43
i_g	--	[2.71, 1.44, 1, 0.74]
r_w	m	0.28
K_b	N·m/MPa	1185
τ_b	sec	0.15
C_A	kg/m	0.2835
f	--	0.02
g	m/s^2	9.81

considered to be rigid and symmetric, without vertical motion, yaw motion, and pitching motion; and 4) the hydraulic braking system is simplified to be a first-order inertial transfer function without pure time delay. Then, the mathematical model of vehicle longitudinal dynamics is

$$\begin{aligned} T_{\rm es} &= \mathbf{MAP}(\omega_e, \alpha_{\rm thr}) \\ T_e &= \frac{1}{\tau_e s+1} T_{\rm es} \\ T_e - T_p &= J_e \dot{\omega}_e \\ T_p &= C_{\rm TC}\omega_e^2,\ T_t = K_{\rm TC} T_p \\ T_d &= \eta_T i_g i_0 T_t,\ \omega_t = i_g i_0 \frac{v}{r_w} \\ M\dot{v} &= \frac{T_d}{r_w} - \frac{T_b}{r_w} - F_i - F_a - F_f \\ T_b &= \frac{K_b}{\tau_b s+1} P_{\rm brk} \\ F_i &= Mg \cdot \mathbf{sin}(\varphi) \\ F_a &= \mathbf{sign}(v+v_{\rm wind}) C_A (v+v_{\rm wind})^2 \\ F_f &= Mg \cdot f \end{aligned} \tag{1}$$

where ω_e is the engine speed, $T_{\rm es}$ is the static engine torque, τ_e is the time constant of engine dynamics, T_e is the actual engine torque, MAP$(\cdot,\cdot)$ is a nonlinear tabular function representing engine torque characteristics, T_p is the pump torque of the TC, J_e is the inertia of fly wheel, T_t is the turbine torque of TC, $C_{\rm TC}$ is the TC capacity coefficient, $K_{\rm TC}$ is the torque ratio of TC, i_g is the gear ratio of transmission, i_0 is the ratio of final gear, η_T is the mechanical efficiency of driveline, r_w is the rolling radius of wheels, M is the vehicle mass, T_d is the driving force on wheels, T_b is the braking force on wheels, v is the vehicle speed, F_i is the longitudinal component of vehicle gravity, F_a is the aerodynamic drag, F_f is the rolling resistance, K_b is the total braking gain of four wheels, τ_b is the time constant of the braking system, C_A is the coefficient of aerodynamic drag, g is the gravity coefficient, f is the coefficient of rolling resistance, φ is the road slope, and $v_{\rm wind}$ is the speed of environmental wind. The nominal values of vehicle parameters are shown in Table I. The characteristic curves of engine torque, TC, and gear-shifting logic are shown in Figs. 3–5, respectively.

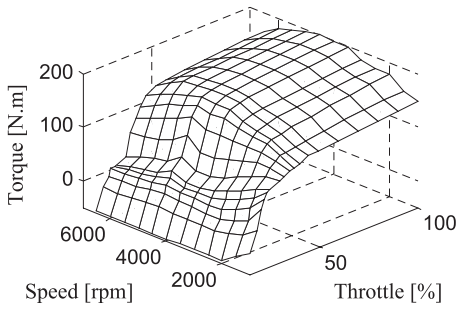

Fig. 3. Engine torque map.

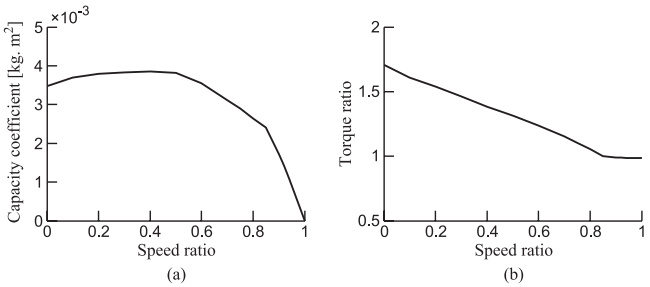

Fig. 4. Characteristics of TC. (a) Capacity coefficient. (b) Torque ratio.

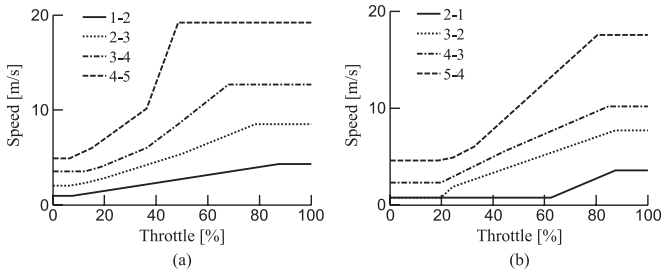

Fig. 5. Switching logic of automated transmission. (a) Shift-up rule. (b) Shift-down rule.

One major challenge of acceleration control is the salient nonlinearities, including engine static nonlinearity, TC coupling, discontinuous gear ratio, quadratic aerodynamic drag, and the throttle/brake switching control. These nonlinearities can be compensated for by the inverse vehicle model, as shown in Fig. 6, (2), shown below, and (3), shown below [24], [33]. The design of the inverse model assumes that 1) engine dynamics and TC coupling are neglected, 2) the vehicle runs on a dry and flat road with no mass transfer, 3) the inverse model uses nominal parameters in Table I. Thus

$$\begin{aligned} T_{\rm edes} &= \frac{r_w}{i_g i_0 \eta_T}(Ma_{\rm des} + C_A v^2 + Mgf) \\ \alpha_{\rm thrdes} &= \mathbf{MAP}^{-1}(\omega_e, T_{\rm edes}) \end{aligned} \tag{2}$$

$$\begin{aligned} F_{\rm bdes} &= Ma_{\rm des} + C_A v^2 + Mgf \\ P_{\rm brkdes} &= \frac{1}{K_b} F_{\rm bdes} \end{aligned} \tag{3}$$

where $a_{\rm des}$ is the input for the inverse model, which is the command of acceleration control, and $T_{\rm edes}$, $\alpha_{\rm thrdes}$, $F_{\rm bdes}$, and $P_{\rm brkdes}$ are the corresponding intermittent variables or

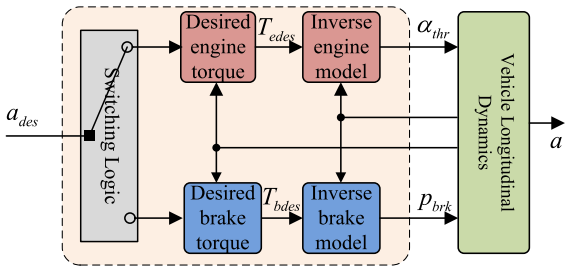

Fig. 6. Inverse model for nonlinearity compensation.

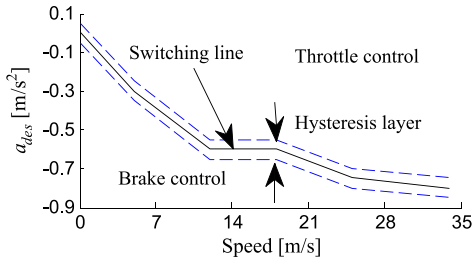

Fig. 7. Switching line between throttle and brake controls.

TABLE II
RANGE OF MAJOR UNCERTAINTIES

	Symbol	Units	Range
Working point v	v	m/s	3~30
Parameters θ	M	kg	800~1600
	η_T	--	0.82~0.92
	τ_e	sec	0.2~0.4
	K_b	Nm/MPa	1100~1250
Disturbances d	φ	rad	-0.15~0.15
	v_{wind}	m/s	-10~10

actuator commands. Note that throttle and braking controls cannot be simultaneously applied. A switching logic with a hysteresis layer is required to determine which control is used. The switching line for separation is not simply to be zero, i.e., $a_{\rm des} = 0$. The engine braking and aerodynamic drag are first used, followed by hydraulic braking if necessary. Therefore, the switching line is actually equal to the deceleration when coasting, as shown in Fig. 7. The use of a hysteresis layer is to avoid frequent switching between throttle and brake controls.

B. Multiple Models to Separate Large Uncertainty

The combination of $\mathbf{I}$ and $\mathbf{V}$ is regarded as the plant for the MMS control. The input of this plant is the desired acceleration $(a_{\rm des})$, and the output is the actual acceleration (a). Its major uncertainties include the change in operating speed, i.e., $v \in \mathbb{R}^1$; the parameter variation, i.e., $\theta = [M, \eta_T, \tau_e, K_b] \in \mathbb{R}^4$; and the external disturbance, i.e., $d = [\varphi, v_{\rm wind}] \in \mathbb{R}^2$. Their uncertain range varies in $v \in [v_{\rm min}, v_{\rm max}]$, $\theta \in [\theta_{\rm min}, \theta_{\rm max}]$, and $d \in [d_{\rm min}, d_{\rm max}]$, as listed in Table II. As previously discussed, such large uncertainties are conflictive with accurate and consistent acceleration tracking. The main idea is to use multiple linear models, i.e., $P_i(s), i = 1, \ldots, N$, to separate large uncertainties

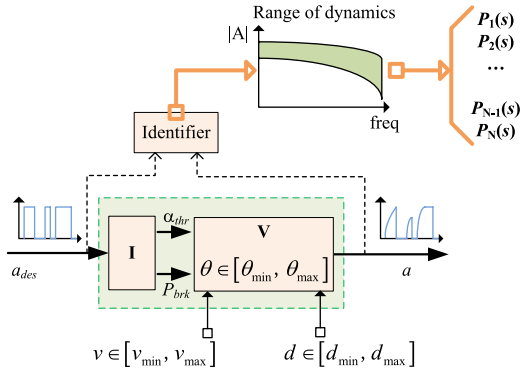

Fig. 8. Procedure to identify multiple models.

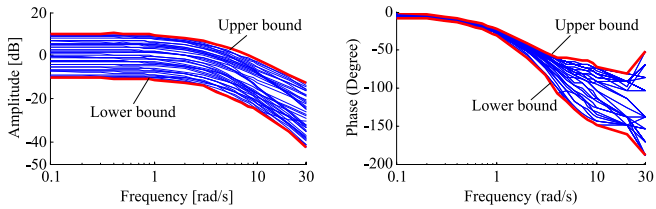

Fig. 9. Identified bode under different setting points.

into small uncertainties and, accordingly, design multiple feasible $\mathbf{H}_\infty$ controllers, i.e., $C_i(s), i = 1, \ldots, N$, for each model with smaller uncertainty.

Fig. 8 shows how to identify $P_i(s), i = 1, \ldots, N$. The identification (by using MATLAB Toolbox ***ident***) is for $\mathbf{V} + \mathbf{I}$, with $\mathbf{I}$ using nominal parameters in Table I and $\mathbf{V}$ using parameters varying in Table II. The range of vehicle speed, i.e., $v \in \mathbb{R}^1$, is equally divided into five points, i.e., $(v_{\rm min}, (3v_{\rm min} + v_{\rm max})/4, (2v_{\rm min} + 2v_{\rm max})/4, (v_{\rm min} + 3v_{\rm max})/4, v_{\rm max})$, and the range of $\theta \in \mathbb{R}^4$ and $d \in \mathbb{R}^2$ are each separated into three points, i.e., $(\theta_{\rm min}, (\theta_{\rm min} + \theta_{\rm max})/2, \theta_{\rm max})$, and $(d_{\rm min}, (d_{\rm min} + d_{\rm max})/2, d_{\rm max})$, respectively. Their combination is set as a candidate for model identification. In total, there are $5 \times 3^{(4+2)} = 3465$ candidate models. Fig. 9 shows the bounds of identified 3465 models (only 30 of them are drawn for conciseness).

The 3465 models can be straightforwardly regarded as a multiple-model set. The shortcoming is easy to see, i.e., models are quite close to each other, which naturally leads to redundant controllers (a waste of computing and storage resources). To reduce the model number, we consider grouping models and covering each group by an uncertain model. Hence, according to the change in system gain, we cluster the 3465 models into four groups and then cover them with four uncertain models $P_i(s), i = 1, \ldots, N$, as shown in Fig. 10.

The model set $\mathbf{P} = \{P_i(s), i = 1, \ldots, N\}$ is selected to share an identical structure with multiplicative uncertainty, i.e.,

$$\begin{aligned} P_i(s) &= G_i(s)\,[1 + \Delta_i W(s)] \\ G_i(s) &= k_{Gi}(s + p_G)^{-1},\ i = 1, \ldots, N \end{aligned} \tag{4}$$

where $G_i(s)$ is the nominal models (listed in Table III), $W(s) = (2.1s + 2.73)(s + 9.5)^{-1}$ is the weight function for

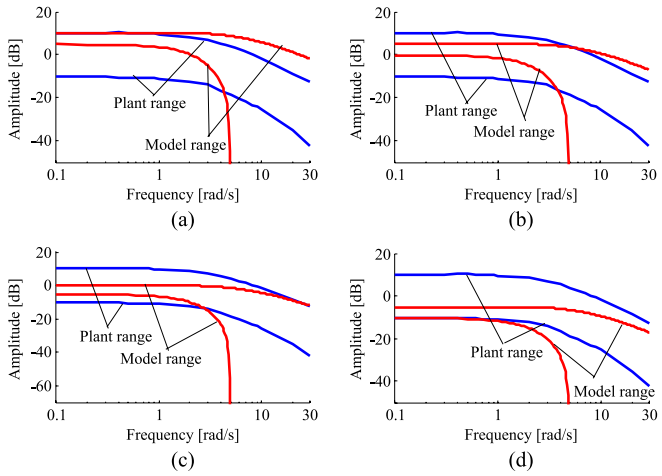

Fig. 10. Bode plot of four linear models. (a) Model $P_1(s)$. (b) Model $P_2(s)$. (c) Model $P_3(s)$. (d) Model $P_4(s)$.

TABLE III
NOMINAL MODEL PARTS

No.	1	2	3	4
$G_i(s)$	$\frac{8.15}{s+3.333}$	$\frac{4.5}{s+3.333}$	$\frac{0.75}{s+3.333}$	$\frac{0.22}{s+3.333}$

uncertainty, and Δ_i is the model uncertainty, satisfying the following equation:

$$\|\Delta_i\|_\infty^\delta < 1, i = 1, \ldots, N \tag{5}$$

where $\|\cdot\|_\infty^{\boldsymbol{\delta}}$ is the induced norm of the $\mathbf{L_2^\delta}$ norm of signals, which is expressed as

$$\|\mathbf{x}(t)\|_{\mathbf{2}}^{\boldsymbol{\delta}} = \sqrt{\int_0^t e^{-\delta(t-\tau)} |\mathbf{x}(t)|^2 \, d\tau} \tag{6}$$

where $\delta > 0$ is the forgetting factor, and $\mathbf{x}(t)$ is the vector of signals.

III. Synthesis of Multiple Model Switching Acceleration Controller

As previously mentioned, the vehicle longitudinal dynamics has relatively large uncertainties because of parametric variation, external disturbances, and unmodeled high-order dynamics. When the modeling mismatch is relatively large, it is challenging to meet the desired requirements of both stability and performance by only using a single $\boldsymbol{H}_\infty$ controller. The main idea of this paper is to use multiple uncertain models to cover the overall plant dynamics and divide the large uncertainty into smaller uncertainties. Here, the 3465 models of vehicle longitudinal dynamics are grouped into four uncertain models. For each uncertain model, a candidate robust controller is designed by solving a set of linear matrix inequalities. Correspondingly, a scheduling logic is employed to select the most proper controller into a closed loop, according to the online measurement or estimation of model errors. This MMS control can largely enhance both robust stability and tracking performance of vehicle acceleration control because it uses an MMS configuration to reduce the range of dynamics covered by each single model. The configuration of MMS control is shown in Fig. 11 [24], [34].

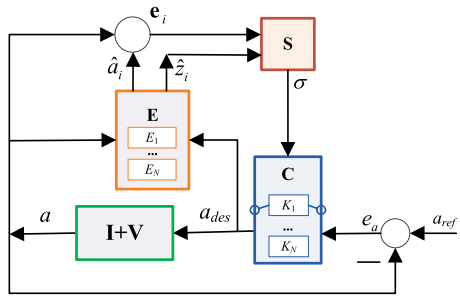

Fig. 11. MMS controller for acceleration tracking control.

The module $\mathbf{E}$ is a set of estimators, which is designed from model set $\mathbf{P}$. Its purpose is to estimate a and z. Note that z is the disturbance signal arising from model uncertainty. The module $\mathbf{S}$ represents the scheduling logic, whose major task is to calculate and compare the switching index of each model J_i $(i = 1, \ldots, N)$. The index J_i actually gives a measure of model uncertainties of each model compared with current vehicle dynamics. The scheduling logic chooses the most proper model (with smallest measure) and denoted as σ. The module $\mathbf{C}$ is a set of $\mathbf{H}_\infty$ controllers, which is also designed from $\mathbf{P}$. The candidate controller whose index is equal to σ will be switched into loop to control acceleration. The signal a_{ref} is the desired acceleration.

A. Design of Switching-Based Control

The scheduling logic is critical to the MMS controller. It evaluates errors between current vehicle dynamics and each model in $\mathbf{P}$ and then determines which controller will be chosen into loop. The controller index σ switched into loop satisfies

$$\sigma = \arg \min_{i=1,\ldots,4} J_i(t). \tag{7}$$

Intuitively, $J_i(t)$ should be designed to measure the amplitude of model uncertainty Δ_i. The estimator set $\mathbf{E} = \{E_i, i = 1, \ldots, N\}$ is used to indirectly measure Δ_i as follows:

$$\begin{aligned} \hat{z}_i &= -\frac{k_{Gi}}{\Lambda(s)} W(s) a_{\text{des}} \\ \hat{a}_i &= \frac{k_{Gi}}{\Lambda(s)} a_{\text{des}} + \frac{\Lambda(s) - (s + p_G)}{\Lambda(s)} a, i = 1, \ldots, 4 \end{aligned} \tag{8}$$

where $\Lambda(s) = 1/(s + 30)$ is the common characteristic polynomial of $\mathbf{E}$, and $\hat{a}_i$ and $\hat{z}_i$ are the estimates of a and z using model P_i. It is easy to know that the stability of the estimator can be ensured by properly selecting $\Lambda(s)$. Subtracting (8) with (4), the estimation error of a becomes

$$e_i = \hat{a}_i - a = -\frac{k_{Gi}}{\Lambda(s)} W(s) \Delta_i a_{\text{des}} = \Delta_i \hat{z}_i. \tag{9}$$

The switching index $J_i(t)$ is designed to be

$$J_i(t) = \left(\|e_i(t)\|_2^\delta \right)^2 - \left(\|\hat{z}_i(t)\|_2^\delta \right)^2, i = 1, \ldots, 4. \tag{10}$$

The controller set $\mathbf{C}$ consists of a group of $\mathbf{H}_\infty$ controllers. Under the MMS structure, $\mathbf{V}+\mathbf{I}$ is covered by $\mathbf{P}$, which has a similar model formulation. Since the system gain from $\hat{z}_\sigma(t)$ to $e_\sigma(t)$ is bounded by properly selected $\mathbf{S}$ (proved in Section III-B), $\hat{z}_\sigma(t)$ and $e_\sigma(t)$ can be treated as the input and output of equivalent uncertainty. Considering (8), $\mathbf{E}$ is rewritten as

$$\begin{aligned}\dot{\mathbf{x}}_E &= \mathbf{A}_E\mathbf{x}_E + \mathbf{B}_{E1}a_{\rm des} + \mathbf{B}_{E2}a\\ \hat{a}_i &= \mathbf{C}_{E1i}\mathbf{x}_E\\ \hat{z}_i &= \mathbf{C}_{E2i}\mathbf{x}_E\end{aligned} \tag{11}$$

where

$$\mathbf{A}_E = \begin{bmatrix} -30 & 0 & & \mathbf{0} \\ 0 & -30 & & \\ & & 0 & -285 \\ \mathbf{0} & & 1 & -39.5 \end{bmatrix},\ \mathbf{B}_{E1} = \begin{bmatrix}1\\0\\1\\0\end{bmatrix}$$

$$\mathbf{B}_{E2} = \begin{bmatrix}0\\1\\0\\0\end{bmatrix}$$

$$\mathbf{C}_{E11} = [8.15 \quad 26.667 \quad \mathbf{0}],\ \mathbf{C}_{E12} = [4.50 \quad 26.667 \quad \mathbf{0}]$$

$$\mathbf{C}_{E13} = [0.75 \quad 26.667 \quad \mathbf{0}],\ \mathbf{C}_{E14} = [0.22 \quad 26.667 \quad \mathbf{0}]$$

$$\mathbf{C}_{E21} = [\mathbf{0} \quad -17.12 \quad 653.79]$$

$$\mathbf{C}_{E22} = [\mathbf{0} \quad -9.45 \quad 360.99]$$

$$\mathbf{C}_{E23} = [\mathbf{0} \quad -1.575 \quad 60.165]$$

$$C_{E24} = [\mathbf{0} \quad -0.462 \quad 17.648].$$

The tracking error $e_a = a_{\rm ref} - a$ is expected to converge to zero. By selecting the weighting function as $W_p(s) = (0.1s + 1.15)/s$, the required tracking performance becomes

$$\|q(t)\|_2^\delta < \gamma \|a_{\rm ref}(t)\|_2^\delta \tag{12}$$

where $a_{\rm ref}$ is the reference acceleration, and $q = W_p(s)(a_{\rm ref} - a)$. Substituting $a = \hat{a}_\sigma - e_\sigma$ and (12) into (11) yields

$$\begin{aligned}\dot{\mathbf{x}} &= \mathbf{A}_\sigma\mathbf{x} + \mathbf{B}_1 e_\sigma + \mathbf{B}_2 a_{\rm des} + \mathbf{B}_3 a_{\rm ref}\\ \hat{z}_\sigma &= \mathbf{C}_{1\sigma}\mathbf{x}\\ q &= \mathbf{C}_{2\sigma}\mathbf{x} + D_p e_\sigma + D_p a_{\rm ref}\\ e_a &= \mathbf{C}_{3\sigma}\mathbf{x} + e_\sigma + a_{\rm ref}\end{aligned} \tag{13}$$

where $C_p = 1.15$, $D_p = 0.1$, $\mathbf{A}_\sigma = \begin{bmatrix}\mathbf{A}_E + \mathbf{B}_{E2}\mathbf{C}_{E1\sigma} & 0\\ -\mathbf{C}_{E1\sigma} & 0\end{bmatrix}$, $\mathbf{B}_1 = \begin{bmatrix}-\mathbf{B}_{E2}\\ -1\end{bmatrix}$, $\mathbf{B}_2 = \begin{bmatrix}\mathbf{B}_{E1}\\ 0\end{bmatrix}$, $\mathbf{B}_3 = \begin{bmatrix}0\\1\end{bmatrix}$, $\mathbf{C}_{1\sigma} = [\mathbf{C}_{E2\sigma} \quad 0]$, $\mathbf{C}_{2\sigma} = [-D_p\mathbf{C}_{E1\sigma} \quad C_p]$, $\mathbf{C}_{3\sigma} = [-\mathbf{C}_{E1\sigma} \quad 0]$, $\mathbf{D}_{31} = 1$, and $\mathbf{x} = \begin{bmatrix}\mathbf{x}_E\\ x_p\end{bmatrix}$.

The $\mathbf{H}_\infty$ controller set is designed by solving linear matrix inequality (LMI) (14), shown at the bottom of the page, where β is a constant smaller than 1. The matrix $\mathbf{A}_{\delta i} = \mathbf{A}_i + 0.5\delta\mathbf{I}$. The symbol "$*$" represents the symmetrical part. The controller set $\mathbf{C}$ is

$$\mathbf{C} = \left\{ K_i : \begin{array}{l}\dot{\mathbf{X}}_C = \mathbf{A}_{Ci}\mathbf{X}_C + \mathbf{B}_{Ci}e_a\\ a_{\rm des} = \mathbf{C}_{Ci}\mathbf{X}_C + \mathbf{D}_{Ci}e_a\end{array},\ i = 1,\ldots,N \right\}. \tag{15}$$

The matrices in (15) are from

$$\begin{aligned}\mathbf{D}_{Ci} &= \tilde{\mathbf{D}}_i\\ \mathbf{C}_{Ci} &= (\tilde{\mathbf{C}}_i - \mathbf{D}_{Ci}\mathbf{C}_{3i}\mathbf{P}_1)(\mathbf{M}^{\mathbf{T}})^{-1}\\ \mathbf{B}_{Ci} &= \mathbf{N}^{-1}(\tilde{\mathbf{B}}_i - \mathbf{P}_2\mathbf{B}_2\mathbf{D}_{Ci})\\ \mathbf{A}_{Ci} &= \mathbf{N}^{-1}\left[\tilde{\mathbf{A}}_i - \mathbf{P}_2(\mathbf{A}_{\delta i} + \mathbf{B}_2\mathbf{D}_{Ci}\mathbf{C}_{3i})\mathbf{P}_1\right](\mathbf{M}^T)^{-1}\\ &\quad - 0.5\delta\mathbf{I} - \mathbf{B}_{Ci}\mathbf{C}_{3i}\mathbf{P}_1(\mathbf{M}^T)^{-1} - \mathbf{N}^{-1}\mathbf{P}_2\mathbf{B}_2\mathbf{C}_{Ci}\\ i &= 1,\ldots,4\end{aligned} \tag{16}$$

where $\mathbf{M}$ and $\mathbf{N}$ are the singular value decomposition of $\mathbf{I} - \mathbf{P}_1\mathbf{P}_2$. The controller set $\mathbf{C}$, which is solved by LMI (14), is listed as follows:

$$\begin{aligned}C &= \{K_1(s), K_2(s), K_3(s), K_4(s)\}\\ K_1(s) &= \frac{137.1(s+4.9)(s+3.133)}{s(s+41.85)(s+45.70)}\\ K_2(s) &= \frac{233.4(s+4.9)(s+3.133)}{s(s+80.06)(s+21.42)}\\ K_3(s) &= \frac{573.0(s+4.9)(s+3.133)}{s(s+29.63)(s+99.30)}\\ K_4(s) &= \frac{283.4(s+4.9)(s+3.133)}{s(s+54.15)(s+19.89)}.\end{aligned} \tag{17}$$

$$\begin{bmatrix} \mathbf{A}_{\delta i}\mathbf{P}_1 + \mathbf{P}_1\mathbf{A}_{\delta i}^T + \mathbf{B}_2\tilde{\mathbf{C}}_i + \tilde{\mathbf{C}}_i^{\mathbf{T}}\mathbf{B}_2^T & * & * & * & * & * \\ \left(\tilde{\mathbf{A}}_i^T + A_{\delta i} + \mathbf{B}_2\tilde{\mathbf{D}}_i\mathbf{C}_{3i}\right)^T & \mathbf{P}_2\mathbf{A}_{\delta i} + \mathbf{A}_{\delta i}^T\mathbf{P}_2 + \tilde{\mathbf{B}}_i\mathbf{C}_{3i} + \mathbf{C}_{3i}^T\tilde{\mathbf{B}}_i^T & * & * & * & * \\ (\mathbf{B}_2\tilde{\mathbf{D}}_i + \mathbf{B}_1)^T & (\mathbf{P}_2\mathbf{B}_1 + \tilde{\mathbf{B}}_i)^{\mathbf{T}} & -\beta^2\mathbf{I} & \mathbf{0} & * & * \\ (\mathbf{B}_2\tilde{\mathbf{D}}_i + \mathbf{B}_3)^T & (\mathbf{P}_2\mathbf{B}_3 + \tilde{\mathbf{B}}_i)^T & \mathbf{0} & -\gamma^2\mathbf{I} & * & * \\ \mathbf{C}_{1i}\mathbf{P}_1 & \mathbf{C}_{1i} & \mathbf{0} & \mathbf{0} & \mathbf{I} & \mathbf{0} \\ \mathbf{C}_{2i}\mathbf{P}_1 & \mathbf{C}_{2i} & D_p & D_p & \mathbf{0} & \mathbf{I} \end{bmatrix} < 0,\ i = 1,\ldots,4$$

$$\begin{bmatrix}\mathbf{P}_1 & \mathbf{I}\\ \mathbf{I} & \mathbf{P}_2\end{bmatrix} > 0 \tag{14}$$

B. Proof of Robust Stability and Robust Performance

Suppose that the switching signal $\sigma(t)$ is

$$\sigma(t)=\begin{cases}\sigma_1,\ 0\le t<t_1\\ \vdots\\ \sigma_n, t_{n-1}\le t<t_n\\ \vdots\end{cases}. \tag{18}$$

Equation (18) means that K_{σ_n} is used when $t_{n-1}\le t<t_n$. From (13) and (15), the closed-loop control system is

$$\begin{aligned}\dot{\mathbf{X}}_{\rm cl}&=\mathbf{A}_{{\rm cl}\sigma}\mathbf{X}_{\rm cl}+\mathbf{B}_{{\rm cl}1\sigma}e_\sigma+\mathbf{B}_{{\rm cl}2\sigma}a_{\rm ref}\\ \hat{z}_\sigma&=\mathbf{C}_{{\rm cl}1\sigma}\mathbf{X}_{\rm cl}\\ q&=\mathbf{C}_{{\rm cl}2\sigma}\mathbf{X}_{\rm cl}+D_pe_\sigma+D_pa_{\rm ref}\\ \sigma&\in\{1,\dots,4\}\end{aligned} \tag{19}$$

where

$$\mathbf{X}_{\rm cl}=\begin{bmatrix}\mathbf{x}\\ \mathbf{X}_C\end{bmatrix},\ \mathbf{A}_{{\rm cl}\sigma}=\begin{bmatrix}\mathbf{A}_\sigma+\mathbf{B}_2\mathbf{D}_{C\sigma}\mathbf{C}_{3\sigma} & \mathbf{B}_2\mathbf{C}_{C\sigma}\\ \mathbf{B}_{C\sigma}\mathbf{C}_{3\sigma} & \mathbf{A}_{C\sigma}\end{bmatrix}$$
$$\mathbf{B}_{{\rm cl}1\sigma}=\begin{bmatrix}\mathbf{B}_1+\mathbf{B}_2\mathbf{D}_{C\sigma}\\ \mathbf{B}_{C\sigma}\end{bmatrix},\ \mathbf{B}_{{\rm cl}2\sigma}=\begin{bmatrix}\mathbf{B}_2\mathbf{D}_{C\sigma}+\mathbf{B}_3\\ \mathbf{B}_{C\sigma}\end{bmatrix}$$
$$\mathbf{C}_{{\rm cl}1\sigma}=[\mathbf{C}_{1\sigma}\quad 0],\ \mathbf{C}_{{\rm cl}2\sigma}=[\mathbf{C}_{2\sigma}\quad 0].$$

Between $[t_{i-1}\ t_i]$, we have

$$\begin{aligned}&e^{-\delta(t-\tau)}\left[|q(\tau)|^2-\gamma^2|a_{\rm ref}(\tau)|^2\right]\\ &\quad=e^{-\delta(t-\tau)}\left[|q(\tau)|^2-\gamma^2|a_{\rm ref}(\tau)|^2+|\hat{z}_{\sigma_i}(\tau)|^2\right.\\ &\qquad\left.-\beta^2|e_{\sigma_i}(t)|^2+\beta^2|e_{\sigma_i}(t)|^2-|\hat{z}_{\sigma_i}(\tau)|^2\right]+\frac{dV[\mathbf{X}_{\rm cl}(\tau)]}{d\tau}\\ &\qquad-\frac{dV[\mathbf{X}_{\rm cl}(\tau)]}{d\tau}\end{aligned} \tag{20}$$

where $V[\mathbf{X}_{\rm cl}(\tau)]=e^{-\delta(t-\tau)}\mathbf{X}_{\rm cl}^T(\tau)\mathbf{P}\mathbf{X}_{\rm cl}(\tau)$ is a Lyapunov function. From (19), we have (21), shown at the bottom of the page.

Substituting (21) into (20) yields (22), shown at the bottom of the page.

Substituting (16) into (14) yields LMI (23), shown at the bottom of the page.

Then, applying the Schur supplement on (23), we have

$$\begin{aligned}&\begin{bmatrix}\left(\mathbf{A}_{\rm cli}+\frac{\delta}{2}\mathbf{I}\right)^T\mathbf{P}+\mathbf{P}\left(\mathbf{A}_{\rm cli}+\frac{\delta}{2}\mathbf{I}\right) & * & *\\ \mathbf{B}_{{\rm cl}1i}^T\mathbf{P} & -\beta^2\mathbf{I} & \mathbf{0}\\ \mathbf{B}_{{\rm cl}2i}^T\mathbf{P} & \mathbf{0} & -\gamma^2\mathbf{I}\end{bmatrix}\\ &\quad+\begin{bmatrix}\mathbf{C}_{{\rm cl}1\sigma_i}^T & \mathbf{C}_{{\rm cl}2\sigma_i}^T\\ \mathbf{0} & D_p^T\\ \mathbf{0} & D_p^T\end{bmatrix}\begin{bmatrix}\mathbf{C}_{{\rm cl}1\sigma_i} & \mathbf{0} & \mathbf{0}\\ \mathbf{C}_{{\rm cl}2\sigma_i} & D_p & D_p\end{bmatrix}<0\\ &i=1,\dots,4.\end{aligned} \tag{24}$$

$$\begin{aligned}|q(\tau)|^2+|\hat{z}_{\sigma_i}(\tau)|^2&=\begin{bmatrix}\mathbf{X}_{\rm cl}\\ e_{\sigma_i}\\ a_{\rm ref}\end{bmatrix}^T\begin{bmatrix}\mathbf{C}_{{\rm cl}1\sigma_i}^T & \mathbf{C}_{{\rm cl}2\sigma_i}^T\\ \mathbf{0} & D_p^T\\ \mathbf{0} & D_p^T\end{bmatrix}\begin{bmatrix}\mathbf{C}_{{\rm cl}1\sigma_i} & \mathbf{0} & \mathbf{0}\\ \mathbf{C}_{{\rm cl}2\sigma_i} & D_p & D_p\end{bmatrix}\begin{bmatrix}\mathbf{X}_{\rm cl}\\ e_{\sigma_i}\\ a_{\rm ref}\end{bmatrix}\frac{dV[\mathbf{X}_{\rm cl}(\tau)]}{d\tau}\\ &=e^{-\delta(t-\tau)}\left[\delta\mathbf{X}_{\rm cl}^T(\tau)\mathbf{P}\mathbf{X}_{\rm cl}(\tau)+\dot{\mathbf{X}}_{\rm cl}^T(\tau)\mathbf{P}\mathbf{X}_{\rm cl}(\tau)+\mathbf{X}_{\rm cl}^T(\tau)\mathbf{P}\dot{\mathbf{X}}_{\rm cl}(\tau)\right]\\ &=e^{-\delta(t-\tau)}\begin{bmatrix}\mathbf{X}_{\rm cl}\\ e_{\sigma_i}\\ a_{\rm ref}\end{bmatrix}^T\begin{bmatrix}\left(\mathbf{A}_{{\rm cl}\sigma_i}+0.5\delta\mathbf{I}\right)^T\mathbf{P}+\mathbf{P}\left(\mathbf{A}_{{\rm cl}\sigma_i}+0.5\delta\mathbf{I}\right) & * & *\\ \mathbf{B}_{{\rm cl}1\sigma_i}^T\mathbf{P} & \mathbf{0} & \mathbf{0}\\ \mathbf{B}_{{\rm cl}2\sigma_i}^T\mathbf{P} & \mathbf{0} & \mathbf{0}\end{bmatrix}\begin{bmatrix}\mathbf{X}_{\rm cl}\\ e_{\sigma_i}\\ a_{\rm ref}\end{bmatrix}\end{aligned} \tag{21}$$

$$\begin{aligned}e^{-\delta(t-\tau)}\left[|q(\tau)|^2-\gamma^2|a_{\rm ref}(\tau)|^2\right]&=e^{-\delta(t-\tau)}\begin{bmatrix}\mathbf{X}_{\rm cl}\\ e_{\sigma_i}\\ a_{\rm ref}\end{bmatrix}^T\left\{\begin{bmatrix}\left(\mathbf{A}_{{\rm cl}\sigma_i}+0.5\delta\mathbf{I}\right)^T\mathbf{P}+\mathbf{P}\left(\mathbf{A}_{{\rm cl}\sigma_i}+0.5\delta\mathbf{I}\right) & * & *\\ \mathbf{B}_{{\rm cl}1\sigma_i}^T\mathbf{P} & -\beta^2\mathbf{I} & \mathbf{0}\\ \mathbf{B}_{{\rm cl}2\sigma_i}^T\mathbf{P} & \mathbf{0} & -\gamma^2\mathbf{I}\end{bmatrix}\right.\\ &\quad\left.+\begin{bmatrix}\mathbf{C}_{{\rm cl}1\sigma_i}^T & \mathbf{C}_{{\rm cl}2\sigma_i}^T\\ \mathbf{0} & D_p^T\\ \mathbf{0} & D_p^T\end{bmatrix}\begin{bmatrix}\mathbf{C}_{{\rm cl}1\sigma_i} & \mathbf{0} & \mathbf{0}\\ \mathbf{C}_{{\rm cl}2\sigma_i} & D_p & D_p\end{bmatrix}\right\}\begin{bmatrix}\mathbf{X}_{\rm cl}\\ e_{\sigma_i}\\ a_{\rm ref}\end{bmatrix}-\frac{dV[\mathbf{X}_{\rm cl}(\tau)]}{d\tau}\\ &\quad+e^{-\delta(t-\tau)}\left[\beta^2|e_{\sigma_i}(t)|^2-|\hat{z}_{\sigma_i}(\tau)|^2\right]\end{aligned} \tag{22}$$

$$\begin{bmatrix}(\mathbf{A}_{\rm cli}+0.5\delta\mathbf{I})^T\mathbf{P}+\mathbf{P}(\mathbf{A}_{\rm cli}+0.5\delta\mathbf{I}) & * & * & * & *\\ \mathbf{B}_{{\rm cl}1i}^T\mathbf{P} & -\beta^2\mathbf{I} & \mathbf{0} & * & *\\ \mathbf{B}_{{\rm cl}2i}^T\mathbf{P} & \mathbf{0} & -\beta^2\mathbf{I} & * & *\\ \mathbf{C}_{{\rm cl}1i} & \mathbf{0} & \mathbf{0} & -\mathbf{I} & \mathbf{0}\\ \mathbf{C}_{{\rm cl}2i} & D_p & D_p & \mathbf{0} & -\mathbf{I}\end{bmatrix}<0, i=1,\dots,4 \tag{23}$$

Integration on both sides of (22) and then from (24) and $\beta < 1$, we have

$$\left(\|q(t)\|_{\mathbf{2}}^{\boldsymbol{\delta}}\right)^2 - \left(\gamma \|a_{\text{ref}}(t)\|_{\mathbf{2}}^{\boldsymbol{\delta}}\right)^2 \leq V\left[\mathbf{X}_{\text{cl}}(0)\right] + \left(\|e_\sigma(t)\|_{\mathbf{2}}^{\boldsymbol{\delta}}\right)^2 - \left(\|\hat{z}_\sigma(t)\|_{\mathbf{2}}^{\boldsymbol{\delta}}\right)^2. \quad (25)$$

For $\forall\, t \in [t_{n-1}\ t_n]$, from (10), we have

$$\left(\|e_\sigma(t)\|_2^\delta\right)^2 - \left(\|\hat{z}_\sigma(t)\|_2^\delta\right)^2 = \left[e^{\delta(t-t_1)} J_{\sigma_1}(t_1)\right] + \cdots + \left[J_{\sigma_n}(t) - e^{\delta(t-t_{n-1})} J_{\sigma_n}(t_{n-1})\right]. \quad (26)$$

Since $J_i(t)$ is continuous w.r.t. t, $J_i(t)$ satisfies (27) at t_i, i.e.,

$$J_{\sigma_i}(t_i) = J_{\sigma_{i+1}}(t_i). \quad (27)$$

Substituting (27) into (26) yields

$$\left(\|e_\sigma(t)\|_2^\delta\right)^2 - \left(\|\hat{z}_\sigma(t)\|_2^\delta\right)^2 = J_{\sigma_n}(t). \quad (28)$$

Considering that $\|\Delta_k\|_\infty^\delta < 1$, we have

$$\|e_k(t)\|_2^\delta \leq \|\hat{z}_k(t)\|_2^\delta. \quad (29)$$

Then, the switching index $J_k(t)$ is limited by

$$J_k(t) = \|e_k(t)\|_2^\delta - \|\hat{z}_k(t)\|_2^\delta \leq 0. \quad (30)$$

Consider (7) and (30), we have

$$\left(\|e_\sigma(t)\|_2^\delta\right)^2 - \left(\|\hat{z}_\sigma(t)\|_2^\delta\right)^2 \leq J_k(t) \leq 0. \quad (31)$$

Substituting (31) into (25), we have

$$\|q(t)\|_{\mathbf{2}}^{\boldsymbol{\delta}} < \gamma \|a_{\text{ref}}(t)\|_{\mathbf{2}}^{\boldsymbol{\delta}} + e^{-0.5\delta t}\sqrt{\varepsilon_1} \quad (32)$$

where $\varepsilon_1 = V[\mathbf{X}_{\text{cl}}(0)]$ is the disturbance from the initial vehicle state. In the sense of exponentially weighted $\mathbf{L}_2$ norm, a_{ref} is attenuated with the level γ and weighting function $W_p(s)$.

IV. Simulation Results and Analyses

For fair comparison, two other controllers are designed, i.e., a sliding mode controller (shorted as SMC) and a single H-inf controller (shorted as Hinf). The SMC is known to have high robustness to matched uncertainties. The design of SMC is based on the nominal model, i.e.,

$$P(s) = \frac{A(s)}{A_{\text{des}}(s)} = \frac{0.33}{s + 0.33}. \quad (33)$$

The sliding surface is designed to be

$$e(t) = a - a_{\text{ref}}$$
$$s = \int_0^t e(t)dt + \lambda e(t) \quad (34)$$

where $\lambda > 0$. The reaching law is selected to be

$$\dot{s} = -ks + \eta \text{sgn}(s) \quad (35)$$

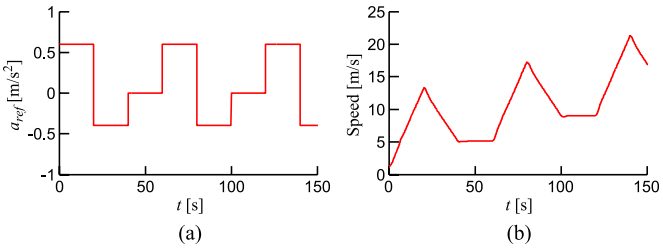

Fig. 12. Reference acceleration and speed profiles. (a) Reference acceleration. (b) Reference speed.

where $k > 0$, and $\lambda > 0$. The sliding mode controller is

$$a_{\text{des}} = \frac{\tau_i}{\lambda k_i}\left[\lambda \dot{a_{\text{ref}}} + \lambda \frac{1}{\tau_i} a - e - ks + \eta \text{sgn}(s)\right]. \quad (36)$$

The H-inf control is another effective approach to handle model uncertainties. A model-matching control structure is applied for better balance between robustness and fastness. The used uncertain model for vehicle dynamics is

$$P(s) = \frac{0.3s + 1}{0.2s^2 + 0.6s + 1}\left(1 + \frac{5.2s + 5}{2s + 10}\right) \|\Delta\|_\infty < 1. \quad (37)$$

The desired acceleration dynamics is

$$G_M(s) = \frac{1}{s + 1}. \quad (38)$$

Then, the feedforward controller designed by the model-matching technique is

$$C_F(s) = \frac{0.2s^2 + 0.6s + 1}{0.3s^2 + 1.3s + 1}. \quad (39)$$

The feedback controller designed by the H-inf control method is

$$C_B(s) = \frac{6.5493(s+5)(s+6)(s^2+3s+5)}{s(s+10.39)(s+4.74)(s^2+7.049s+14.03)}. \quad (40)$$

This H-inf controller is solved by the MATLAB command mixsyn(). The weighting function for robust performance is $W_p(s) = (0.1s + 1.15)s^{-1}$. Two profiles of reference acceleration are used in comparison: 1) periodic stepping acceleration [see Fig. 12(a) and (b)] and 2) naturalistic acceleration from real traffic flow [see Fig. 14(a)]. Two groups of simulations are conducted for each acceleration profile: 1) nominal condition; and 2) uncertain condition. For the nominal condition, all vehicle parameters are shown in Table I, with no road slope and wind. For the uncertain condition, three main factors change, including vehicle mass, road slope, and wind. The vehicle mass uses its maximum value, i.e., $M = 1600$ kg; the disturbance of road slope is sinusoidal signal. Thus

$$\varphi = \varphi_{\max} \cdot \sin\left(\frac{2}{T_{\text{slope}}} t\right) \quad (41)$$

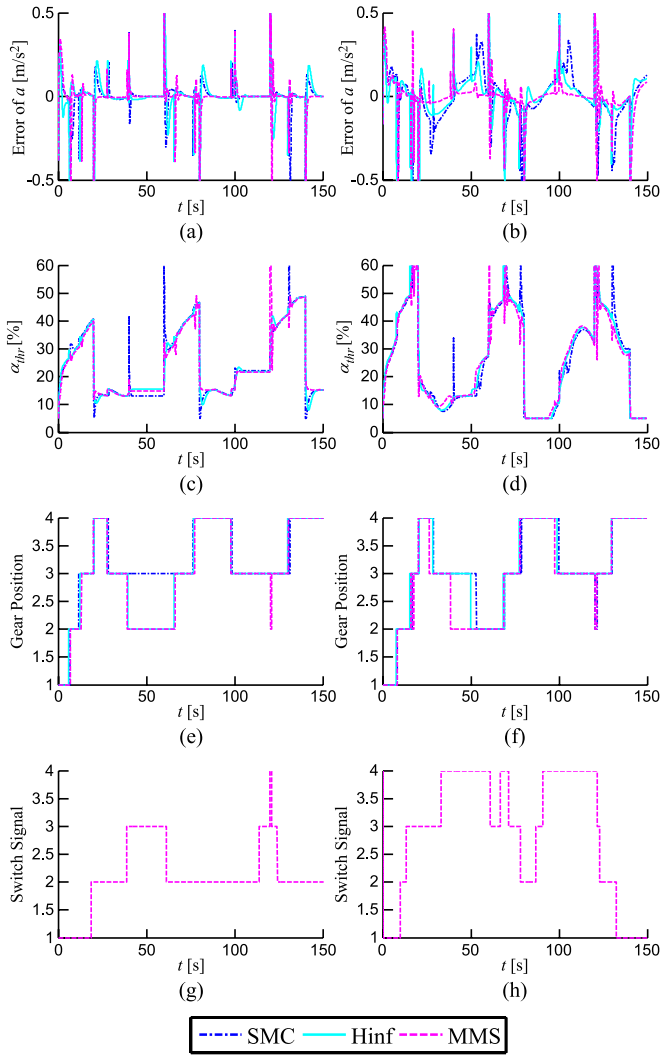

Fig. 13. Results of the periodic stepping acceleration profile. (a) Nominal. (b) Uncertain. (c) Nominal. (d) Uncertain. (e) Nominal. (f) Uncertain. (g) Nominal. (h) Uncertain.

where $\varphi_{\max} = 5^{\deg}$ and $T_{\text{slope}} = 50$ s. The disturbance of wind is periodic triangular signal, i.e.,

$$v_{\text{wind}} = 2\frac{v_{\text{wmax}}}{T_{\text{wind}}}t - v_{\text{wmax}},\ t \in [0, T_{\text{wind}}) \tag{42}$$

where $v_{w\max} = 10$ m/s, and $T_{\text{wind}} = 40$ s.

A. Case 1: Periodic Stepping Acceleration

The periodic stepping acceleration profiles have a period of 60 s, in which the reference acceleration first steps into 0.6 m/s^2, then drops to -0.4 m/s^2, and finally goes back to zero. Fig. 13 shows the simulation results. In the nominal condition, all three controllers track the reference acceleration accurately without steady-state errors. The SMC and Hinf have somewhat higher overshoots. With uncertainties, the tracking capability of SMC and Hinf decreases with obvious tracking errors, whereas MMS is capable of ensuring small tracking errors. In the nominal condition, MMS tends to use controllers 2 and 3, whereas MMS in the uncertain condition tends to use more

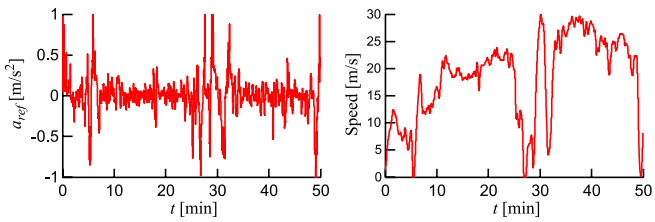

Fig. 14. Reference acceleration and speed profiles.

of controller 4 [see Fig. 13(g) and (h)]. This selection by MMS is reasonable because of the increase in vehicle mass in the uncertain condition. The increase in mass will reduce the system gain (tends to use model 4 in Table III), thus leading to the use of high-numbered controllers. Another concern that must be explained is the spike of acceleration. This is mainly caused by the impact of powertrain when the gear switches. A more appropriately designed transmission model could improve the gear-shifting quality.

In addition, both gear shift and controller switch can cause spikes in throttle angle and acceleration. Take the time span from 60 to 75 s in the uncertain condition as an example. In Fig. 13(d), from 60 to 75 s, there are three spikes in throttle angle in the uncertain condition. It can be seen that the first spike in throttle angle (around 61 s) is caused by the controller switch from No. 4 to No. 3. The second spike (69 s) is caused by the gear shift-up from gear 2 to gear 3, and the third spike (around 80 s) is a combined effect of gear shift-up (from gear 3 to gear 4) and control switching (from No. 3 to No. 2).

B. Case 2: Acceleration Profile From Naturalistic Traffic Flow

The naturalistic acceleration profile is from driver experiment data, which lasts around 50 min in total [see Fig. 14(b)]. The simulation results are shown in Fig. 15 (only from 0 to 500 s as a demonstration). The results are similar to those with periodic stepping acceleration, in which MMS performs the best in the uncertain condition. In MMS, the usage of controllers is also similar. As the vehicle mass increases, high-numbered controllers are used more frequently.

A more deep simulation is conducted in Fig. 16, in which the level of uncertainty is increased step by step. The relationship of the number of uncertain levels (denoted by symbol i) with model uncertainties is shown as follows:

$$\begin{aligned} M &= 1200\text{ kg} + 40\text{ kg} \cdot i \\ \varphi_{\max} &= 1\text{ deg} \cdot i \\ v_{w\max} &= 2\text{ m/s} \cdot i \end{aligned} \tag{43}$$

where i represents the level of uncertainty, with the maximum mass of 1600 kg, maximum road slope of 10 deg, and maximum environmental wind of 20 m/s (when $i = 10$). When $i = 0$, there is no model uncertainty. Fig. 16 presents the root mean square error (RMSE) of acceleration error and the number of gear shifting per minute (denoted as $N_{\text{gear}}/\min$). In the nominal condition, the RMSE of tracking error is almost identical for the three controllers; as the uncertainty level increases, SMC

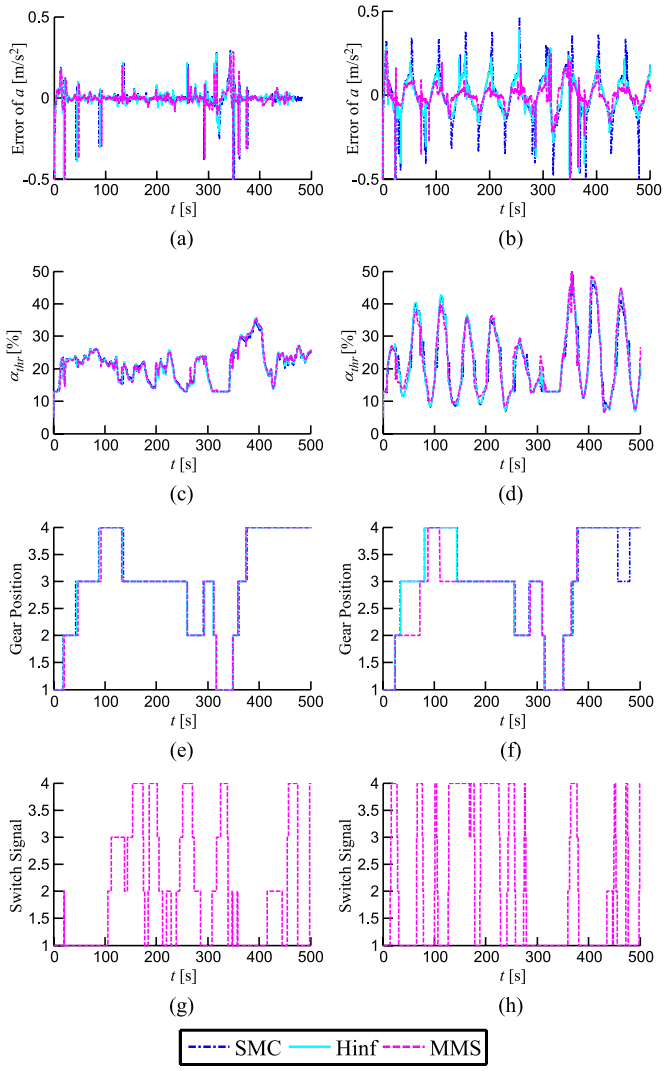

Fig. 15. Results of naturalistic acceleration profile. (a) Nominal. (b) Uncertain. (c) Nominal. (d) Uncertain. (e) Nominal. (f) Uncertain. (g) Nominal. (h) Uncertain.

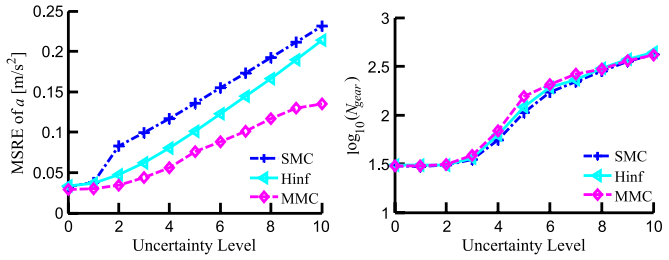

Fig. 16. Performance comparisons under different uncertain levels.

and Hinf quickly drop acceleration tracking performance while MMS still holds best accuracy. Fig. 16(b) is used to release the concern that MMS might largely increase the number of gear shifting due to its switching structure.

V. Experimental Tests

The MMS control is further validated through field tests with a passenger car. As shown in Fig. 17, the experimental platform is built based on a passenger car with identical parameters as in

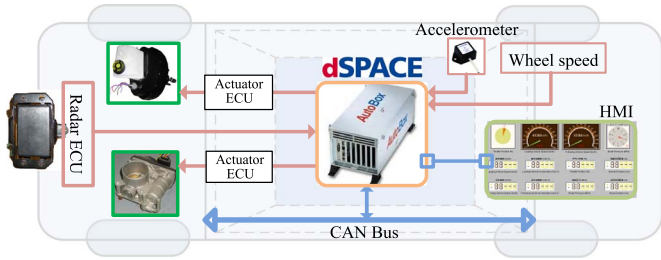

Fig. 17. System configuration of test vehicles.

(a) (b)

Fig. 18. Test scenarios. (a) Test scenario on a flat road. (b) Test scenario on a down slope.

simulation. The millimeter-wave radar is equipped to detect a frontal moving target. Two actuators, i.e., an electronic throttle and an electronic vacuum booster, are used to execute control commands. The dSPACE controller runs the MMS control algorithm. Moreover, dSPACE also fulfills other functions, including radar signal processing, target vehicle selection, inverse model calculation, and communication with CAN bus. The signals, such as throttle opening and brake pressure, are broadcasted through CAN bus and recorded by a dSPACE controller. Some test scenarios are shown in Fig. 18.

The validation tests were done under two conditions: nominal condition and uncertain condition. At the nominal condition, the test road is flat, and the vehicle is loaded at its nominal weight. The nominal condition has two tests: 1) acceleration control and 2) deceleration control. Desired acceleration stays at 0 m/s^2 during the first 7 s and then goes to either 0.8 m/s^2 (for the acceleration control test) or -0.8 m/s^2 (for the deceleration control test) as a step signal filtered by a first-order transfer function [see Figs. 19(a) and 20(a)]. The desired acceleration finally goes to 0 m/s^2 after 8 s. The test results are shown in Figs. 19 and 20, respectively. The test results show that under MMS control, actual acceleration tracks the desired value as expected, and the maximum tracking error is smaller than 0.15 m/s^2. During the acceleration control test, the controller switches from 2 to 3 at about 15 s, which means that during 7–15 s, $P_2(s)$ is closet to real vehicle dynamics; after 15 s, $P_3(s)$ describes vehicle dynamics better. During the deceleration control test, no controller switching occurs [see Fig. 19(b)]. It must be noted that the throttle is not closed fully when the vehicle decelerates between 7 and 16 s, as shown in Fig. 20(c), because the engine still needs a certain amount of fresh air to maintain idling.

In an uncertain condition, the disturbances arise from varying road slope (around $\pm 3^\circ$) and increased mass change (with two more passengers, around plus 120 kg). The test results are shown in Fig. 21. In Fig. 21(a), actual vehicle acceleration

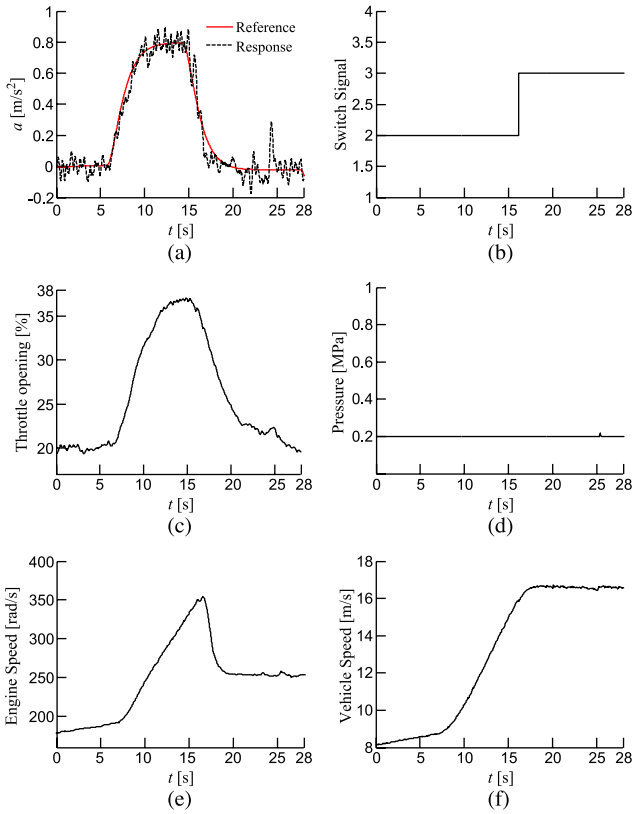

Fig. 19. Acceleration control under normal conditions. (a) Acceleration. (b) Switch signal. (c) Throttle opening. (d) Braking pressure. (e) Engine speed. (f) Vehicle speed.

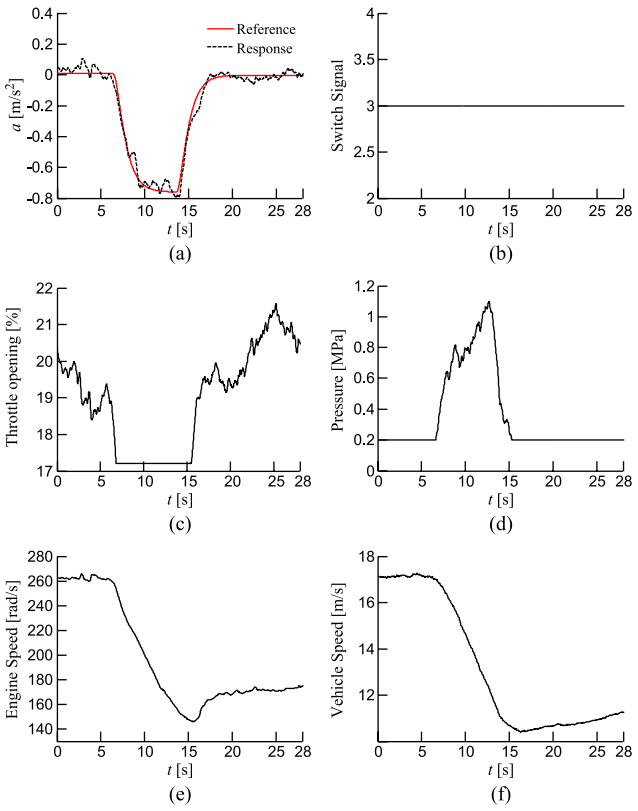

Fig. 20. Deceleration control under nominal conditions. (a) Acceleration. (b) Switch signal. (c) Throttle opening. (d) Braking pressure. (e) Engine speed. (f) Vehicle speed.

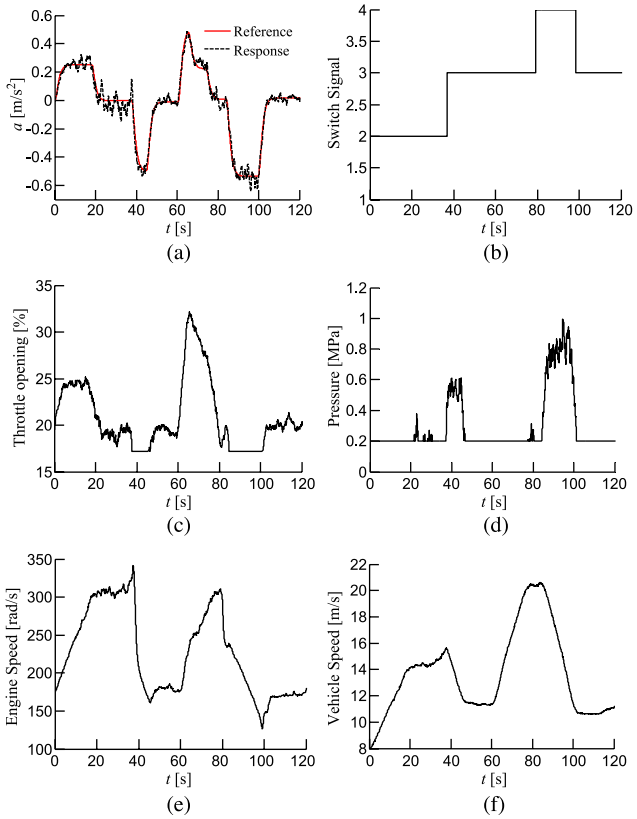

Fig. 21. Acceleration control under the uncertain conditions. (a) Acceleration. (b) Switch signal. (c) Throttle opening. (d) Braking pressure. (e) Engine speed. (f) Vehicle speed.

tracks the desired value as expected. Although external resistance force and vehicle load differs from the nominal value, the maximum tracking error is still smaller than 0.15 m/s^2. Compared with the experimental results under nominal conditions, the disturbances arising from environmental and vehicle parameters are greatly attenuated, and the vehicle tracks the reference acceleration finely. The vehicle combined with its acceleration controller acts closely to the required dynamics. Then, the vehicle node in the platoon can be considered to have the same dynamics called homogeneous, which can simplify the design of a platoon control system. Furthermore, although switching results in some sudden changes in control input during simulation, in practical use, the throttle opening and braking pressure act smoothly, even at switching time.

VI. Conclusion

This paper has proposed a new robust acceleration tracking control of vehicle longitudinal dynamics for the purpose of platoon-level automation. The design, which is based on an MMS control structure, is able to offer more consistent and approximately linear node dynamics for upper-level control design even under large uncertainties, including vehicle parametric variation, varying road slope, and strong environmental wind. The following remarks are concluded.

1) The platoon control strongly necessitates homogeneous and linear node dynamics, which requires the acceleration tracking performance to be accurate and consistent. This requirement is rather challenging because of the

linearization error of powertrain dynamics and large model uncertainties in and around vehicles. The MMS control structure divides the large uncertainties of vehicle longitudinal dynamics into small uncertainties, then designs multiple $\mathbf{H}_\infty$ controllers from the multiple-model set, and automatically selects the most appropriate candidate into loop according to the errors between current vehicle dynamics and multiple models.

2) The designed switching index can measure the model error of vehicle longitudinal dynamics properly, and the right acceleration controller is selected into closed loop. The robust stability and performance of this acceleration tracking control system is ensured by the small gain theorem. The combined simulation and experiment results demonstrate that this switching control system has enhanced performance than that designed by either the H-infinity or sliding mode control approach in large-uncertainty conditions.

REFERENCES

[1] T. Luettel, M. Himmelsbach, and J. Wuensche, "Autonomous ground vehicles—Concepts and a path to the future," *Proc. IEEE 100*, pp. 1831–1839, May 2012.

[2] X. Huang and Y. Fang, "Performance study of node-disjoint multipath routing in vehicular ad hoc networks," *IEEE Trans. Veh. Technol.*, vol. 58, no. 4, pp. 1942–1950, May 2009.

[3] S. Shladover, "Longitudinal control of automotive vehicles in close-formation platoons," *Trans. ASME, J. Dyn. Syst. Meas. Control*, vol. 113, no. 2, pp. 231–241, Jun. 1991.

[4] S. Sheikholeslam and C. Desoer, "Longitudinal control of a platoon of vehicles with no communication of lead vehicle information: A system level study," *IEEE Trans. Veh. Technol.*, vol. 42, no. 4, pp. 546–554, Nov. 1993.

[5] J. Hedrick, M. Tomizuka, and P. Varaiya, "Control issues in automated highway systems," *IEEE Trans. Control Syst.*, vol. 14, no. 6, pp. 21–32, Dec. 1994.

[6] R. Rajamani *et al.*, "Design and experimental implementation of longitudinal control for a platoon of automated vehicles," *Trans. ASME, J. Dyn. Syst. Meas. Control*, vol. 12, no. 3, pp. 470–476, Jun. 2000.

[7] J. Wang and R. Rajamani, "Should adaptive cruise control systems be designed to maintain a constant time-gap between vehicles," *IEEE Trans. Veh. Technol.*, vol. 53, no. 5, pp. 1480–1490, Sep. 2004.

[8] J. Wang and R. Longoria, "Coordinated and reconfigurable vehicle dynamics control," *IEEE Trans. Control Syst. Technol.*, vol. 17, no. 3, pp. 723–732, May 2009.

[9] P. Ioannou and C. Chien, "Autonomous intelligent cruise control," *IEEE Trans. Veh. Technol.*, vol. 42, no. 4, pp. 657–672, Nov. 1993.

[10] S. Stankovic, M. Stanojevic, and D. Siljak, "Decentralized overlapping control of a platoon of vehicles," *IEEE Trans. Control Syst. Technol.*, vol. 8, no. 5, pp. 816–832, Sep. 2000.

[11] R. Rajamani and S. Shladover, "An experimental comparative study of autonomous and cooperative vehicle following control systems," *Transp. Res. C, Emerging Technol.*, vol. 9, no. 1, pp. 15–31, Feb. 2001.

[12] P. Barooah, P. Mehta, and J. Hespanha, "Mistuning-based control design to improve closed-loop stability margin of vehicular platoons," *IEEE Trans. Autom. Control*, vol. 54, no. 9, pp. 2100–2113, Sep. 2009.

[13] H. Hao and P. Barooah, "Stability and robustness of large platoons of vehicles with double-integrator models and nearest neighbor interaction," *Int. J. Robust Nonlinear Control*, vol. 23, no. 18, pp. 2097–2122, Dec. 2013.

[14] S. Eben Li, K. Li, and J. Wang, "Economy oriented vehicle adaptive cruise control with coordinating multiple objectives function," *Veh. Syst. Dyn.*, vol. 51, no. 1, pp. 1–17, Jan. 2013.

[15] S. Eben Li, K. Li, R. Rajamani, and J. Wang, "Model predictive multi-objective vehicular adaptive cruise control," *IEEE Trans. Control Syst. Technol.*, vol. 19, no. 3, pp. 556–566, May 2011.

[16] Z. Chen, C. Mi, J. Xu, X. Gong, and C. You, "Online energy management for a power-split plug-in hybrid electric vehicle based on dynamic programming and neural network," *IEEE Trans. Veh. Technol.*, vol. 63, no. 4, pp. 1567–1580, May 2014.

[17] M. Zhang, Y. Yang, and C. Mi, "Analytic system optimization and test verification for an idealized parallel ICE-electric powertrain," *IEEE Trans. Veh. Technol.*, vol. 61, no. 4, pp. 1554–1566, May 2012.

[18] A. Fritz and W. Schiehlen, "Automatic cruise control of a mechatronically steered vehicle convoy," *Veh. Syst. Dyn.*, vol. 32, no. 4/5, pp. 331–344, Nov. 1999.

[19] A. Fritz and W. Schiehlen, "Nonlinear ACC in simulation and measurement," *Veh. Syst. Dyn.*, vol. 36, no. 2/3, pp. 159–177, Sep. 2001.

[20] K. Hunt, T. Johansen, and J. Kalkkuhl, "Speed control design for an experimental vehicle using a generalized gain scheduling approach," *IEEE Trans. Control Syst. Technol.*, vol. 8, no. 3, pp. 381–395, May 2000.

[21] D. Swaroop, J. Hedrick, and S. Choi, "Direct adaptive longitudinal control of vehicle platoons," *IEEE Trans. Veh. Technol.*, vol. 17, no. 1, pp. 150–161, Jan. 2001.

[22] A. Higashimata and K. Adachi, "Design of a headway distance control system for ACC," *JSAE Rev.*, vol. 22, no. 1, pp. 15–22, Jan. 2001.

[23] Y. Yamamura and Y. Seto, "An ACC design method for achieving both string stability and ride comfort," *J. Syst. Des. Dyn.*, vol. 2, no. 4, pp. 979–990, Jan. 2008.

[24] F. Gao and K. Li, "Hierarchical switching control of longitudinal acceleration with large uncertainties," *Int. J. Autom. Tech.*, vol. 8, no. 3, pp. 351–359, 2007.

[25] Z. Xu and P. Ioannou, "Adaptive throttle control for speed tracking," *Veh. Syst. Dyn.*, vol. 23, no. 1, pp. 293–306, Jan. 1994.

[26] J. Keneth, A. Tor, and K. Jens, "Speed control design for an experimental vehicle using a generalized scheduling approach," *IEEE Trans. Control Syst. Technol.*, vol. 8, no. 3, pp. 381–395, May 2000.

[27] J. Naranjo, C. Gonzalez, and R. Carcia, "ACC+stop&go maneuvers with throttle and brake fuzzy control," *IEEE Trans. Intell. Transp. Syst.*, vol. 7, no. 2, pp. 213–225, Jun. 2006.

[28] X. Dai, C. Li, and A. Rad, "An approach to tune fuzzy controllers based on reinforcement learning for autonomous vehicle control," *IEEE Trans. Intell. Transp. Syst.*, vol. 6, no. 3, pp. 285–293, Sep. 2005.

[29] J. Hespanha, D. Liberzon, and A. Morse, "Hysteresis-based switching algorithms for supervisory control of uncertain systems," *Automatica*, vol. 39, no. 2, pp. 263–272, Feb. 2003.

[30] J. Hespanha, D. Liberzon, and A. Morse, "Multiple model adaptive control. Part 2: Switching," *Int. J. Robust Nonlinear Control*, no. 11, no. 5, pp. 479–496, Apr. 2001.

[31] X. Rong, Z. Zhao, and X. Li, "General model set design methods for multiple model approach," *IEEE Trans. Autom. Control*, vol. 50, no. 9, pp. 1260–1276, Sep. 2005.

[32] P. Bashivan and A. Fatehi, "Improved switching for multiple model adaptive controller in noisy environment," *J. Process Control*, vol. 22, no. 2, pp. 390–396, Feb. 2012.

[33] R. Kianfar, B. Augusto, and A. Ebadighajari, "Design and experimental validation of a cooperative driving system in the grand cooperative driving challenge," *IEEE Trans. Intell. Transp. Syst.*, vol. 13, no. 3, pp. 994–1007, Sep. 2012.

[34] F. Gao, S. E. Li, D. Kum, and H. Zhang, "Synthesis of multiple model switching controllers using $\mathbf{H}_\infty$ theory for system with large uncertainties," *Neurocomputing*, vol. 157, pp. 118–124, Jun. 2015.

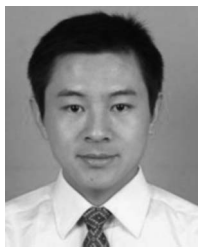

Shengbo Eben Li (M'13) received the M.S. and Ph.D. degrees from Tsinghua University, Beijing, China, in 2006 and 2009, respectively.

He was with Stanford University, Stanford, CA, USA, in 2007; the University of Michigan, Ann Arbor, MI, USA, from 2009 to 2011; and the University of California at Berkeley, Berkeley, CA, in 2015. He is currently an Associate Professor with the Department of Automotive Engineering, Tsinghua University. He is the author of about 80 journal/conference papers and the coinventor of over 20 patents. His active research interests include autonomous vehicle control, driver behavior and assistance, battery control for electric vehicles/hybrid electric vehicles, and optimal control and multiagent control.

Dr. Li received the Distinguished Doctoral Dissertation of Tsinghua University (2009), the National Award for Technological Invention in China (2013), the Best Student Paper Award at the 2014 IEEE Intelligent Transportation System Symposium, and the Best Paper Award at the 14th Intelligent Transport System Asia-Pacific Forum.

Feng Gao received the M.S. degree in vehicle engineering and the Ph.D. degree in mechanical engineering from Tsinghua University, Beijing, China, in 2003 and 2007, respectively.

From February 2007 to February 2013, he was a Senior Engineer with the Changan Auto Global R&D Center, where he has led several key industrial projects involving electromagnetic compatibility, durability test of electronic modules, advanced driver-assistance systems, and engine control. Since February 2013, he has been a Professor with Chongqing University, Chongqing, China. His current research interests include robust control, optimization, and multiple-model approach with application to vehicle systems.

Dongpu Cao received the Ph.D. degree from Concordia University, Montréal, QC, Canada, in 2008.

He is currently a Lecturer with the Center for Automotive Engineering, Cranfield University, Cranfield, U.K. His research focuses on vehicle dynamics, control, and intelligence, on which he has contributed more than 80 publications and one U.S. patent.

Dr. Cao received the Best Paper Award at the 2010 ASME International Conference on Advanced Vehicle and Tire Technologies and the 2012 SAE Arch T. Colwell Merit Award. He serves as an Associate Editor for the IEEE TRANSACTIONS ON INTELLIGENT TRANSPORTATION SYSTEMS, the IEEE TRANSACTIONS ON VEHICULAR TECHNOLOGY, and the IEEE TRANSACTIONS ON INDUSTRIAL ELECTRONICS. He has been a Guest Editor for *Vehicle System Dynamics*, the IEEE/ASME TRANSACTIONS ON MECHATRONICS, and the IEEE TRANSACTIONS ON HUMAN–MACHINE SYSTEMS. He serves on the SAE International Vehicle Dynamics Standards Committee and on several ASME, SAE, and IEEE technical committees.

Keqiang Li received the B.Tech. degree from Tsinghua University, Beijing, China, in 1985 and the M.S. and Ph.D. degrees from Chongqing University, Chongqing, China, in 1988 and 1995, respectively.

He is currently a Professor of automotive engineering with Tsinghua University. He has authored over 90 papers and is a coinventor on 12 patents in China and Japan. His main areas of research interest include vehicle dynamics and control for driver-assistance systems and hybrid electrical vehicles.

Dr. Li is a Senior Member of the Society of Automotive Engineers of China and has served on the Editorial Board of the *International Journal of ITS Research* and the *International Journal of Vehicle Autonomous Systems*. He has received the "Changjiang Scholar Program Professor" award, as well as several other awards from public agencies and academic institutions in China.